Scanning Tunneling and Atomic Force Microscopy Study of the Te-Atom Surfaces of Commensurate Layered Tellurides NbA_xTe_2 (A = Ge, Si)

W. Liang and M.-H. Whangbo*

Department of Chemistry, North Carolina State University, Raleigh, North Carolina 27695-8204

M. Evain, L. Monconduit, and R. Brec*

Laboratoroire de Chimie des Solides, Institut des Matêriaux de Nantes, Universitê de Nantes, 44072 Nantes Cedex 03, France

H. Bengel, H.-J. Cantow, and S. N. Magonov*

Materials Research Center (F.M.F.), Albert-Ludwigs University, Stefan-Meier-Strasse 31A, D-79104 Freiburg, Germany

Received December 20, 1993. Revised Manuscript Received March 7, 1994®

The surfaces of commensurate layered tellurides $NbGe_{2/5}Te_2$, $NbGe_{1/3}Te_2$, and $NbSi_{1/2}Te_2$ were examined by scanning tunneling microscopy (STM) and atomic force microscopy (AFM). The observed atomic-resolution STM and AFM images were analyzed in terms of the partial and total electron density plots of their surfaces calculated by the extended Hückel tight-binding electronic band structure method. The STM and AFM images of these phases are characterized by a pseudohexagonal arrangement of spots representing the surface Te atoms, and the surface unit-cell parameters of these commensurate MA_xTe_2 phases are well reproduced by STM and AFM. The atomic size patterns of the AFM and STM images differ in their relative contrasts from those expected on the basis of the surface Te-atom corrugations. This discrepancy is explained if the surface Te-atom sheets undergo a slight height reconstruction, most likely because the short interlayer Te···Te contacts present in the bulk crystals are truncated at the surface.

Introduction

The ternary tellurides MA_xTe_2 (M = Nb, Ta; A = Si, Ge) are made up of [Te/M,A/Te] sandwich layers, in which the M and A atoms reside in the trigonal prismatic and square-planar coordination sites, respectively.[1–4] These compounds adopt commensurate superstructures when x takes rational values, and incommensurate superstructures otherwise. Commensurate superstructures reported are $NbSi_{1/2}Te_2$,[3] $MA_{1/3}Te_2$ (M = Nb, A = Ge; M = Nb, A = Si; M = Ta, A = Si),[2] $NbGe_{2/5}Te_2$,[1] and $NbGe_{3/7}Te_2$.[4] So far, one incommensurate structure has been characterized (i.e., $TaSi_{0.360}Te_2$).[5] Figure 1 shows that, in terms of the zigzag chains a, b, and c of trigonal prisms, the sandwich layers of the commensurate MA_xTe_2 phases are written as $(ab)_nc$ (n = 1, 2, 3, etc.), where the chains a and b contain M–M pairs and A atoms while chain c contains isolated M atoms. Thus, the general formulas of the commensurate MA_xTe_2 phases are given by $MA_{n/(2n+1)}Te_2$. [$NbSi_{1/2}Te_2$ results when $n = \infty$, i.e., its sandwich layers are made up of the chains a and b only.][6] This description of the commensurate phases led to the suggestion[1] that incommensurate MA_xTe_2 phases may result when their sandwich layers have nonuniform distributions of the chains a, b, and c [e.g., $\cdots(ab)_2c(ab)_3c(ab)c\cdots$]. This kind of incommensurate structure is difficult to determine with high accuracy (i.e., to get precise coordinates and thus bond distances) even with space groups beyond the traditional three-dimensional ones. It may be possible to detect such an incommensurate phase by the local-probe methods scanning tunneling microscopy (STM) and atomic force microscopy (AFM).[7] To demonstrate the feasibility of this approach, one should be able to identify by STM and AFM the surface unit cells of the commensurate MA_xTe_2 phases whose crystal structures are well-known.

In STM the image contrast is determined by the variation of the tunneling current between the tip and surface, and the image is simulated by the *partial* electron density of the surface, $\rho(r_0,e_f)$ (i.e., the electron density associated with the energy levels in the vicinity of the Fermi level and evaluated at the tip position r_0).[8] In the

® Abstract published in *Advance ACS Abstracts*, April 1, 1994.

(1) van der Lee, A.; Evain, M.; Mansuetto, M.; Monconduit, L.; Brec, R.; Rouxel, J. *J. Solid State Chem.*, in press.
(2) (a) Li, J.; Caroll, P. J. *Mater. Res. Bull.* **1992**, *27*, 1073. (b) Monconduit, L.; Evain, M.; Boucher, F.; Brec, R.; Rouxel, J. *Z. Anorg. Allg. Chem.* **1992**, *616*, 1. (c) Li, J.; Badding, E.; DiSalvo, F. J. *J. Alloys Comp.* **1992**, *184*, 257. (d) Evain, M.; Monconduit, L.; van der Lee, A.; Brec, R.; Rouxel, J.; Canadell, E. *New J. Chem.*, in press.
(3) (a) Monconduit, L.; Evain, M.; Brec, R.; Rouxel, J.; Canadell, E. *C. R. Acad. Sci. Paris* **1993**, *314*, 25. (b) Canadell, E.; Monconduit, L.; Evain, M.; Brec, R.; Rouxel, J.; Whangbo, M.-H. *Inorg. Chem.* **1992**, *32*, 10.
(4) van der Lee, A.; Evain, M.; Monconduit, L.; Brec, R.; Smaalen, S. *J. Phys.: Condens. Mater.*, in press.
(5) van der Lee, A.; Evain, M.; Monconduit, L.; Brec, R.; Rouxel, J.; Petricek, V. *Acta Crystallogr. B*, in press.

(6) In terms of the (MTe_2) and (M_2Te_2) units containing the isolated M and the M–M dimer, respectively, MA_xTe_2 phases can be written as $(M_2Te_2)_{0.5-y}(A)_{0.5-y}(MTe_2)_{2y}$ with $x = 0.5 - y$.
(7) For recent reviews, see: *Scanning Tunneling Microscopy I, II, III*; Guntherodt, H.-J, Wiesendanger, R., Eds.; Springer-Verlag: Heidelberg, 1992–1993.

0897-4756/94/2806-0678$04.50/0 © 1994 American Chemical Society

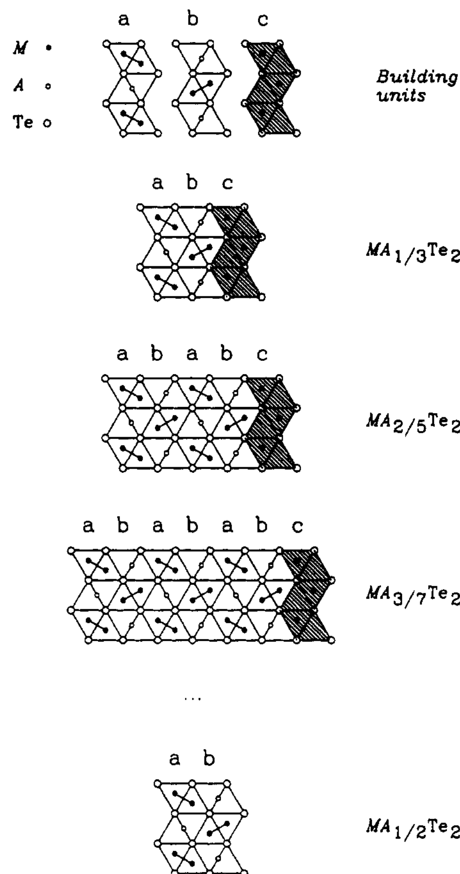

Figure 1. Top projection views of the sandwich layers of commensurate MA_xTe_2 phases in terms of the building units, the zigzag chains (a, b, and c) made up of MTe_6 trigonal prisms. The chain c contains isolated M atoms, while the chains a and b contain M–M pairs.

Table 1. Rectangular Unit-Cell Parameters (nanometers) of the Surface Te-Atom Sheets of $NbGe_{2/5}Te_2$, $NbGe_{1/3}Te_2$, and $NbSi_{1/2}Te_2$ Determined from X-ray Crystal Structures and from AFM and STM Images

compound	parameter	X-ray	AFM	STM
$NbGe_{2/5}Te_2$	*a*	0.644	0.68 ± 0.05	0.65 ± 0.06
	c	1.947	2.00 ± 0.10	1.90 ± 0.10
$NbGe_{1/3}Te_2$	*a*	0.646	0.66 ± 0.03	0.62 ± 0.03
	c	1.169	1.11 ± 0.06	1.12 ± 0.06
$NbSi_{1/2}Te_2$	*b*	0.7888	0.83 ± 0.04	0.85 ± 0.07
	c	0.6336	0.63 ± 0.04	0.64 ± 0.04

contact mode AFM the image contrast is governed by the variation of primarily the repulsive interactions between the tip and surface, and the image is described by the *total* electron density of the surface, $\rho(r_0)$.[9] Recently, the STM and AFM images of various layered chalcogenides and halides[10] have successfully been interpreted in terms of the $\rho(r_0,e_f)$ and $\rho(r_0)$ plots calculated by the extended Hückel tight-binding (EHTB) electronic band structure method.[11]

In the present work, we examine the surfaces of three commensurate tellurides $NbGe_{2/5}Te_2$, $NbGe_{1/3}Te_2$, and

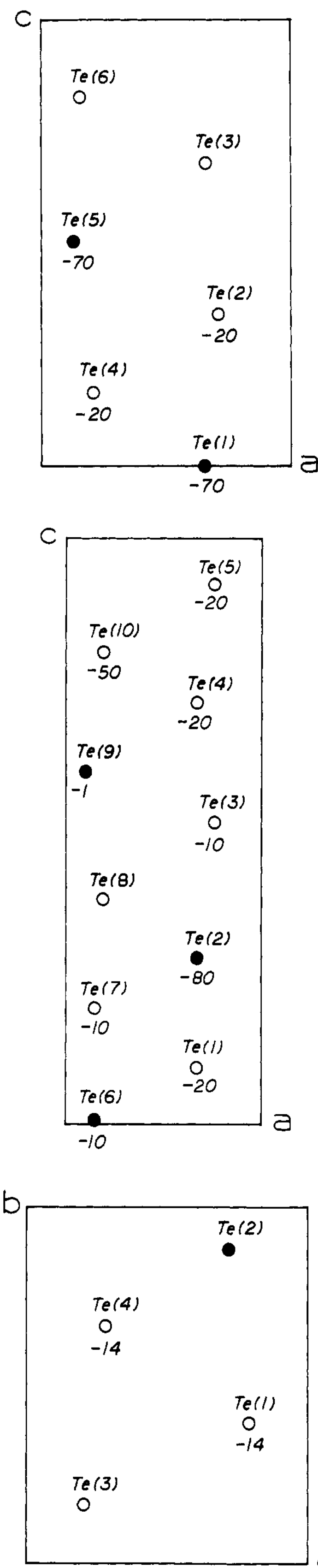

Figure 2. Surface Te atom arrangements in the sandwich layers of (a, top) $NbGe_{2/5}Te_2$, (b, middle) $NbGe_{1/3}Te_2$, and (c, bottom) $NbSi_{1/2}Te_2$, where the Te atoms represented by circles. The Te atoms making the shortest interlayer Te···Te contacts are shown by filled circles. The number around each atom represents the relative height in milliangstroms with respect to the most protruded surface Te atoms. The latter are Te(8) in $NbGe_{2/5}Te_2$, Te(3) and Te(6) in $NbGe_{1/3}Te_2$, and Te(2) and Te(3) in $NbSi_{1/2}Te_2$.

(8) Tersoff, J.; Hamman, D. R. *Phys. Rev. B* **1985**, *31*, 805.
(9) Meyer, E.; Heinzelmann, H. in ref 6 (Vol. II, p 99, 1992).
(10) (a) Parkinson, B. A.; Ren, J.; Whangbo, M.-H. *J. Am. Chem. Soc.* **1991**, *113*, 7833. (b) Ren, J.; Whangbo, M.-H.; Bengel, H.; Magonov, S. N. *J. Phys. Chem.* **1993**, *97*, 4764. (c) Magonov, S. N.; Zönnchen, P.; Rotter, H.; Thiele, G.; Cantow, H.-J.; Ren, J.; Whangbo, M.-H. *J. Am. Chem. Soc.* **1993**, *115*, 2495. (d) Whangbo, M.-H.; Ren, J.; Canadell, E.; Louder, D.; Parkinson, B. A.; Bengel, H.; Magonov, S. N. *J. Am. Chem. Soc.* **1993**, *115*, 3760.
(11) Whangbo, M.-H.; Hoffmann, R. *J. Am. Chem. Soc.* **1978**, *100*, 6093.

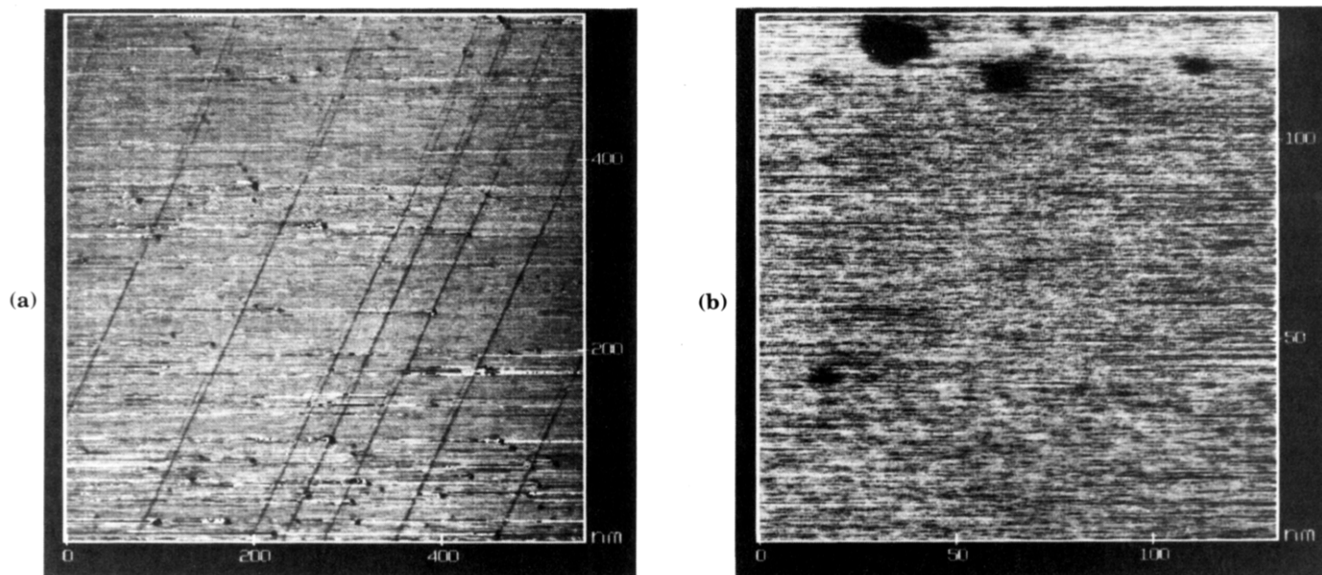

Figure 3. (a) Large-scale STM image recorded for the *ac* plane of $NbGe_{2/5}Te_2$ (I_{tun} = 9 nA, V_{bias} = 30 mV). The contrast covers the height variations in the 0.0–2.0-nm range. (b) Large-scale AFM image recorded for the *ac* plane of $NbGe_{1/3}Te_2$. The contrast covers the height variations in the 0.0–2.0-nm range.

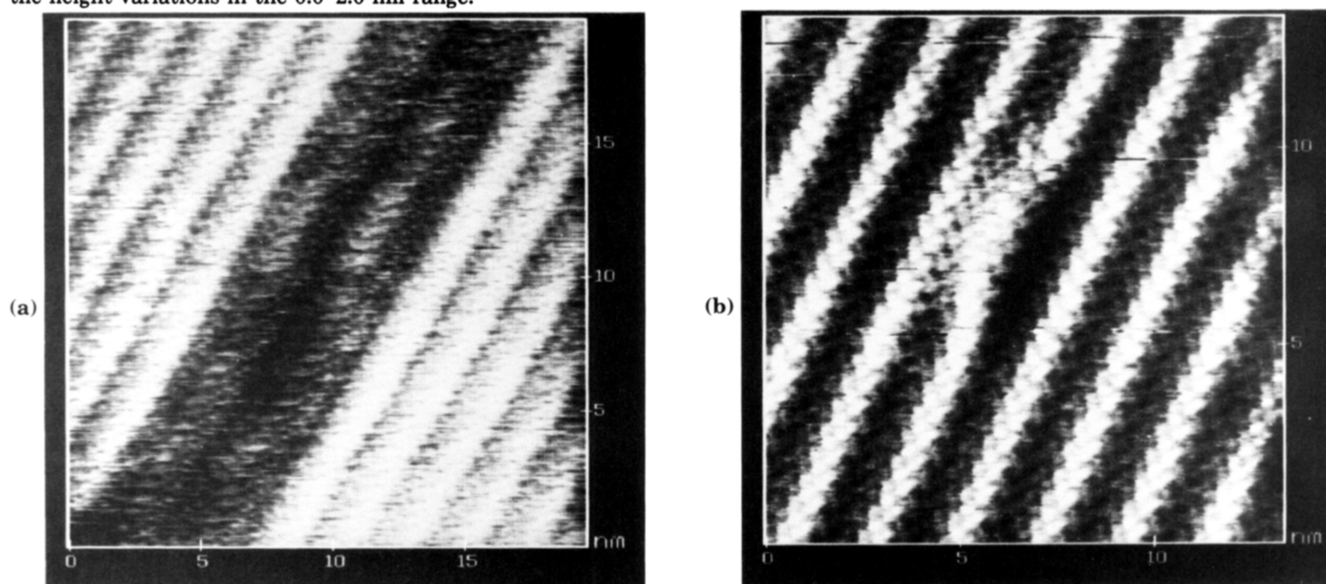

Figure 4. STM images recorded for the *ac* plane of $NbGe_{2/5}Te_2$ (I_{tun} = 9 nA, V_{bias} = 30 mV) in (a) and (b). The contrast covers the height variations in the 0.0–1.0-nm range in (a) and in the 0.0–0.6-nm range in (b).

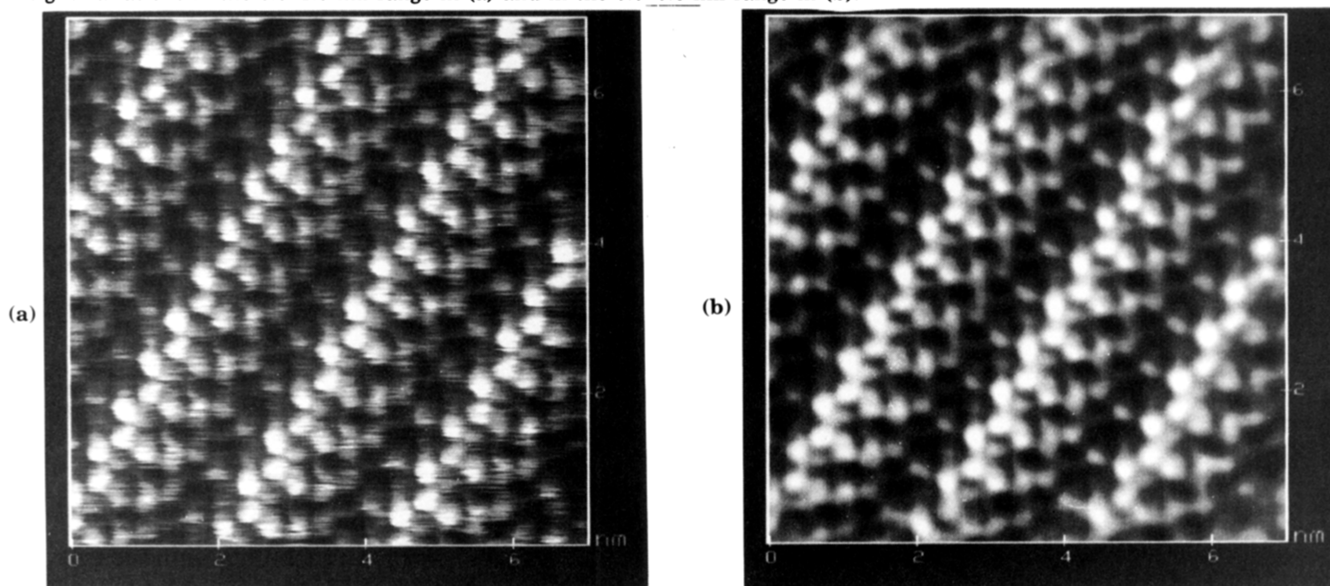

Figure 5. STM height image recorded for the *ac* plane of $NbGe_{2/5}Te_2$ (I_{tun} = 6.9 nA, V_{bias} = −31 mV): (a) unfiltered and (b) filtered. The contrast covers the height variations in the 0.0–0.5-nm range.

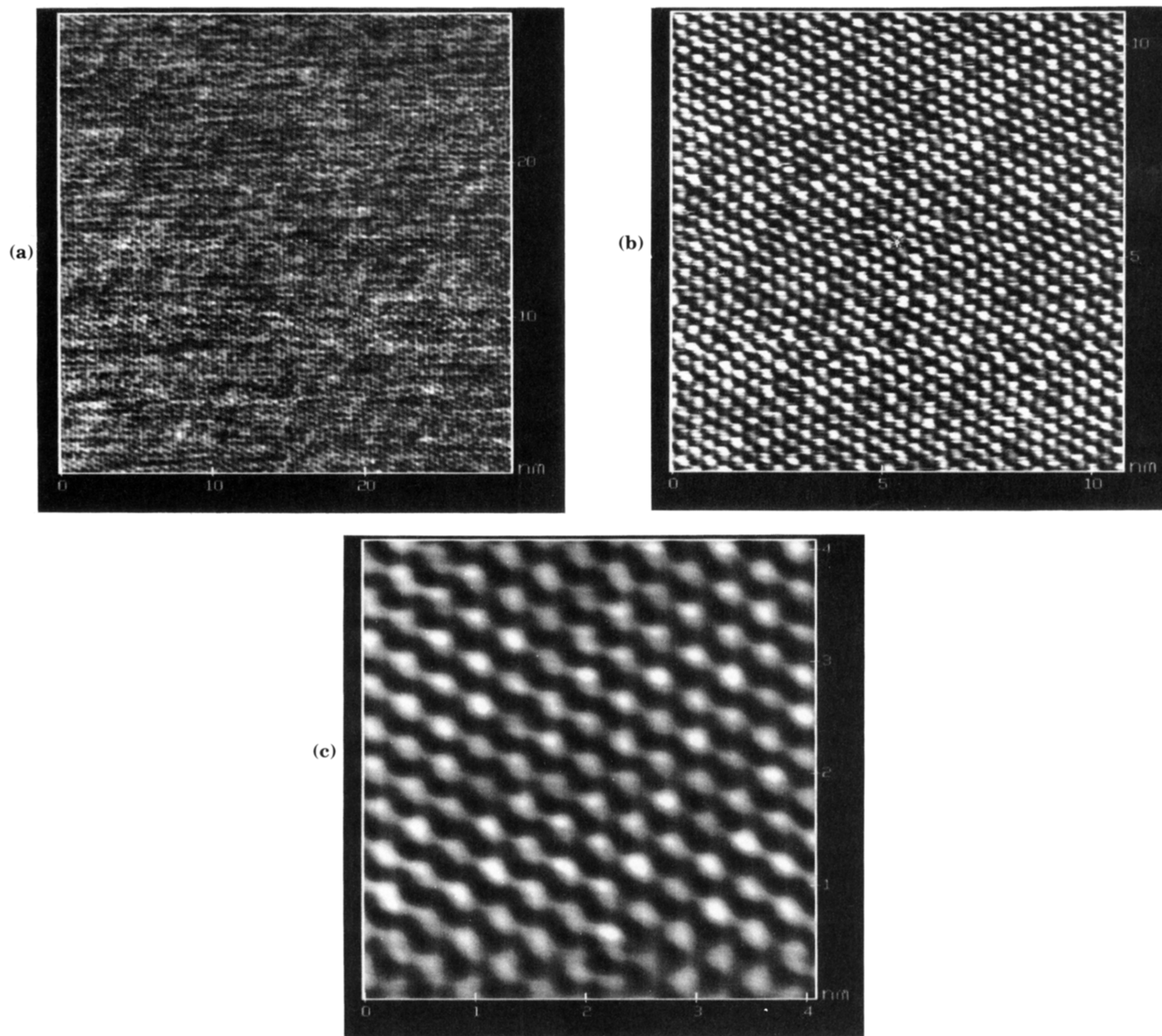

Figure 6. (a) AFM image recorded for the *ac* plane of $NbGe_{2/5}Te_2$. The contrast covers height variations in the 0–2-nm range. (b) AFM image recorded for the *ac* plane of $NbGe_{2/5}Te_2$. The contrast covers height variations in the 0.0–1.5-nm range. (c) Zoomed part of the image in (b) after FFT filtering.

$NbSi_{1/2}Te_2$ by STM and AFM. The atomic-resolution STM and AFM images of these compounds are then analyzed by calculating their $\rho(r_0,e_f)$ and $\rho(r_0)$ plots on the basis of the EHTB electronic band structure method.

Experimental Section

Ambient condition STM and AFM measurements were conducted by employing a commercial scanning probe microscope, Nanoscope II (Digital Instruments, Inc.), with a mechanically sharpened Pt/Ir wire as the STM tip and a Si_3N_4 pyramidal probe as the AFM tip. Measurements were made on freshly cleaved surfaces of the crystal samples because, after several hours spent at ambient conditions, their surfaces were covered with some kind of adsorbates. To improve the periodic features of the atomic scale images, some of them were filtered with the fast Fourier transform (FFT) procedure: only the most pronounced frequency peaks of the power spectrum were chosen to restore the idealized image with the reverse transform. Other details of the STM and AFM experiments can be found elsewhere.[10,12] For $NbGe_{2/5}Te_2$ and $NbGe_{1/3}Te_2$, the STM images do not depend on the polarity of the bias voltages (V_{bias}), thereby suggesting that they are metals. For $NbSi_{1/2}Te_2$, stable STM images are obtained only for positive V_{bias}, thereby indicating that it is a semiconductor. Indeed, EHTB electronic band structure calculations show that $NbGe_{1/3}Te_2$ and $NbGe_{2/5}Te_2$ are metals, and $NbSi_{1/2}Te_2$ is a semiconductor. Thus, the $\rho(r_0,e_f)$ plots of $NbGe_{1/3}Te_2$ and $NbGe_{2/5}Te_2$ can be calculated by using the band orbitals having the energy e lying within the energy window $|e - e_f| = 4k_BT$ (at room temperature, $4k_BT = 0.1$ eV). Our calculations show that the $\rho(r_0,e_f)$ plots calculated with several different energy windows (0.125 eV and smaller) are essentially identical. $NbSi_{1/2}Te_2$ is deficient in Si, i.e., the coefficient for Si is actually less than 0.5. Within a rigid-band approximation, the electronic structure of this Si-deficient phase, $NbSi_{(1/2-\delta)}Te_2$ ($\delta > 0$), can be approximated by that of $NbSi_{1/2}Te_2$ by removing 4δ electrons per Si from the top of its valence band. Then, for the STM imaging of $NbSi_{(1/2-\delta)}Te_2$ with $V_{bias} > 0$, the electron from the tip flows into the valence band top rather than the conduction band bottom. Therefore, the $\rho(r_0,e_f)$ plot for $NbSi_{1/2}Te_2$, which will stand for $NbSi_{(1/2-\delta)}Te_2$ hereafter, was calculated by employing the energy levels lying within 0.25 eV from the top of the valence band. Here again, the $\rho(r_0,e_f)$ plots with different energy window smaller than 0.25 eV are essentially identical. In the calculations of the $\rho(r_0,e_f)$ and $\rho(r_0)$ plots, the tip–surface distance r_0 wastaken to be 1.5 Å from the most protruded surface Te atoms. Other details of our calculations are described elsewhere.[10,12]

(12) Magonov, S. N.; Whangbo, M.-H. *Adv. Mater.*, in press.

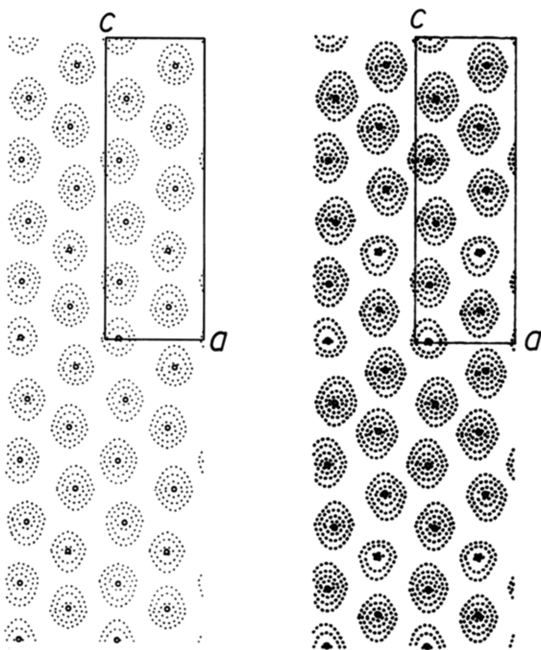

Figure 7. (a, left) $\rho(r_0)$ plot calculated for the *ac* plane of $NbGe_{2/5}Te_2$. The contour values are 0.18, 0.10, and 0.05 × 10^{-1} electron/au^3. (b, right) $\rho(r_0,e_f)$ plot calculated for of the *ac* plane $NbGe_{2/5}Te_2$. The contour values are 0.30, 0.20, 0.10, and 0.05 × 10^{-3} electron/au^3.

Surface Structures

Figure 2 shows projection views of the surface Te sheets of the sandwich layers in $NbGe_{2/5}Te_2$, $NbGe_{1/3}Te_2$, and $NbSi_{1/2}Te_2$, and their surface unit cell parameters are listed in Table 1. All these surface sheets exhibit a pseudohexagonal arrangement of Te atoms. The number around each Te atom represents the relative height as derived from the bulk crystal structures. In general, the height corrugation in the surface Te sheets is not strong: the maximum height difference in the surface Te atoms is 0.10 Å in $NbGe_{2/5}Te_2$, 0.07 Å in $NbGe_{1/3}Te_2$, and 0.01 Å in $NbSi_{1/2}Te_2$. The three compounds have interlayer Te···Te contacts much shorter than the van der Waals radii sum (4 Å). The Te atoms involved in the shortest interlayer Te···Te contacts (3.743 Å in $NbGe_{2/5}Te_2$, 3.787 Å in $NbGe_{1/3}Te_2$, and 3.759 Å in $NbSi_{1/2}Te_2$) are indicated by filled circles in Figure 2.

Large-Scale Images

As shown in Figure 3a for $NbGe_{2/5}Te_2$, large-scale STM images show dark linear and dark grainlike imperfections. The grainlike defects, observed at plus and minus V_{bias}, are assigned to domains of missing surface atoms because similar defects are also found in the AFM images of both compounds. The AFM image of $NbGe_{1/3}Te_2$ in Figure 3b shows dark spots with linear dimensions of 7–15 nm, which are the smallest defects found in our AFM experiments. Periodic features of atomic resolution are detected by AFM, but unlike the case of STM images, reliable AFM images demonstrating atomic-site defects have not been found.

At a higher magnification, the STM image of $NbGe_{2/5}Te_2$ (Figure 4a) shows periodic rows with fine substructures. The repeat distance of these rows along the direction perpendicular to them is 2.0 ± 0.1 nm, which coincides with the crystallographic *c* parameter. The missing rows in the center of Figure 4a form a groove with depth of ca. 0.4 nm, i.e., the thickness of one $NbGe_{2/5}Te_2$ layer. The darker patterns within the linear groove are assigned to the underlying layer. Such linear defects as found in the STM images have not been observed by AFM. Figure 4b shows another imperfection of the STM image in a bent pattern.

Atomic-Scale Images and Density Plots

Common Features. Atomic-scale STM images of $NbGe_{2/5}Te_2$, $NbGe_{1/3}Te_2$, and $NbSi_{1/2}Te_2$ are shown in Figures 5, 8, and 11, respectively, and atomic-scale AFM images of $NbGe_{2/5}Te_2$, $NbGe_{1/3}Te_2$, and $NbSi_{1/2}Te_2$ are shown in Figures 6, 9, and 12, respectively. All these STM and AFM images consist of atomic-size spots of varying contrasts to form periodic patterns consisting of bright and dim rows (along the *a*-axis direction for $NbGe_{2/5}Te_2$ and $NbGe_{1/3}Te_2$ and along the *c*-axis direction for $NbSi_{1/2}Te_2$). If the intensity differences are neglected, the bright spots form a pseudohexagonal pattern in both

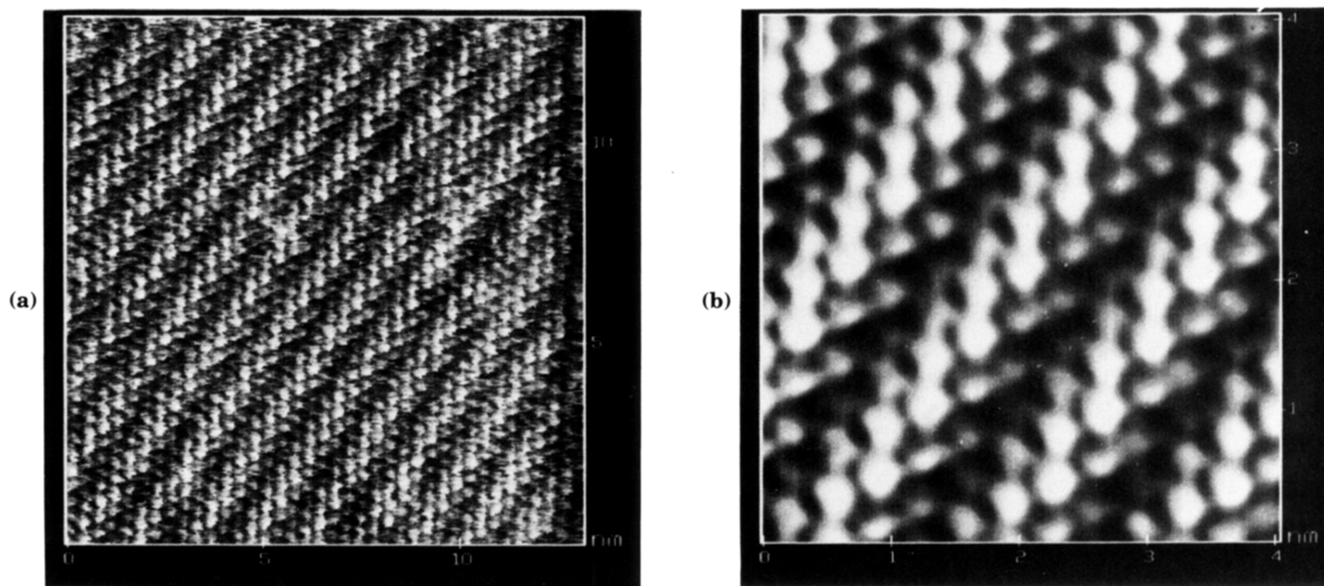

Figure 8. (a) STM height image recorded for the *ac* plane of $NbGe_{1/3}$ (I_{tun} = 3 nA, V_{bias} = 60 mV). The contrast covers the height variations in the 0.0–1.4-nm range. (b) Zoomed part of (b), where the contrast covers the height variations in the 0.0–1.0-nm range.

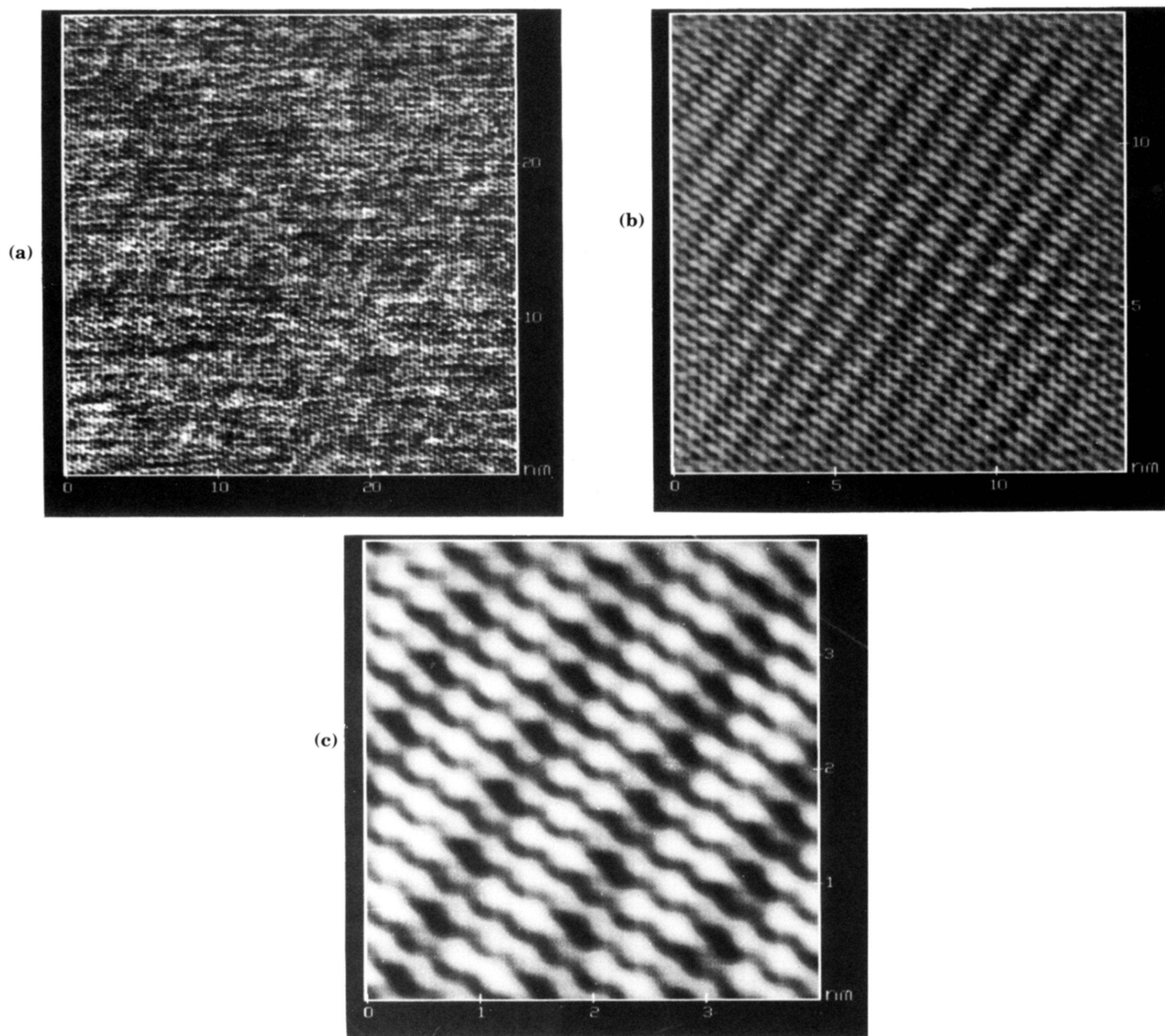

Figure 9. (a) AFM height image recorded for the *ac* plane of $NbGe_{1/3}Te_2$. The contrast covers height variations in the 0–1-nm range. (b) Part of the image (a) after FFT filtering. The contrast covers height variations in the 0–1-nm range. (c) Zoomed part of (b). The contrast covers height variations in the 0–1-nm range.

the STM and AFM images. As summarized in Table 1, the surface unit cell parameters determined from the STM and AFM images are in good agreement with the corresponding values expected from the bulk crystal structures. The $\rho(r_0,e_f)$ and $\rho(r_0)$ plots calculated for single sandwich layers of $NbGe_{2/5}Te_2$, $NbGe_{1/3}Te_2$, and $NbSi_{1/2}Te_2$ are shown in Figures 7, 10, and 13, respectively. In all these plots, the electron density representing each surface Te atom is centered at the atomic position so that, as expected from the surface atom positions (Figure 2), the Te-atom density patterns form a pseudohexagonal arrangement when the intensity differences are neglected. This explains why the bright spots of the STM and AFM images are arranged in a similar way.

Specific Features. *$NbGe_{2/5}Te_2$.* Of the 10 surface Te atoms of a unit cell, both Te(6) and Te(2) are lower lying than the remaining ones (Figure 2a), and these atoms have lower electron densities in the $\rho(r_0)$ plot (Figure 7a). Note that Te(6) and Te(2) are not adjacent. In the AFM image (Figure 6b), however, there is a zigzag pattern of dim spots, although the contrast difference between these spots and the rest is not strong. This can be explained if there is a slight height reconstruction in the surface Te-atom sheet. The spots of the STM images (Figure 5) show much greater contrast differences than do those of the AFM images. According to the $\rho(r_0,e_f)$ plot (Figure 7b), 8 of the 10 Te atoms of a unit cell should have comparable contributions to the image. However, in the STM image, there are only five to six bright spots per unit cell Figure 5.

$NbGe_{1/3}Te_2$. According to the bulk crystal structures, the surface Te-atom corrugation is weaker in $NbGe_{1/3}Te_2$ than in $NbGe_{2/5}Te_2$ (Figure 2). Nevertheless, the AFM image of $NbGe_{1/3}Te_2$ (Figure 9) shows a much stronger corrugation than does that of $NbGe_{2/5}Te_2$ (Figure 6). Three of the six spots per unit cell are brighter than the remaining ones, so that chains of bright spots alternate with chains of dim spots along the *c*-axis direction. The contrast differences between the bright and dim spots are much larger than expected from the $\rho(r_0)$ plot (Figure 10a) or the surface atom corrugation (Figure 2b). This suggests a slight height reconstruction in the surface Te-atom sheet. Note that the patterns of the STM image (Figure 8) is quite similar to those of the AFM image (Figure 9), and the $\rho(r_0,e_f)$ plot (Figure 10b) based on the bulk crystal structure does not reproduce the occurrence of alternating contrast variations in the STM image (Figure 8). The

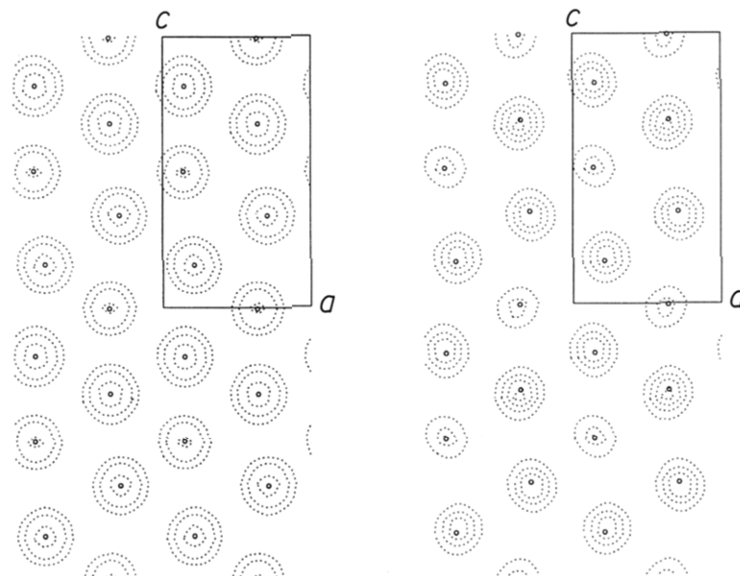

Figure 10. (a, left) $\rho(r_0)$ plot calculated for the *ac* plane of $NbGe_{1/3}Te_2$. The contour values are 0.20, 0.10, and 0.05 × 10^{-1} electron/au^3. (b, right) $\rho(r_0,e_f)$ plot calculated for the *ac* plane of $NbGe_{1/3}Te_2$. The contour values are 0.40, 0.30, 0.20, and 0.10 × 10^{-3} electron/au^3.

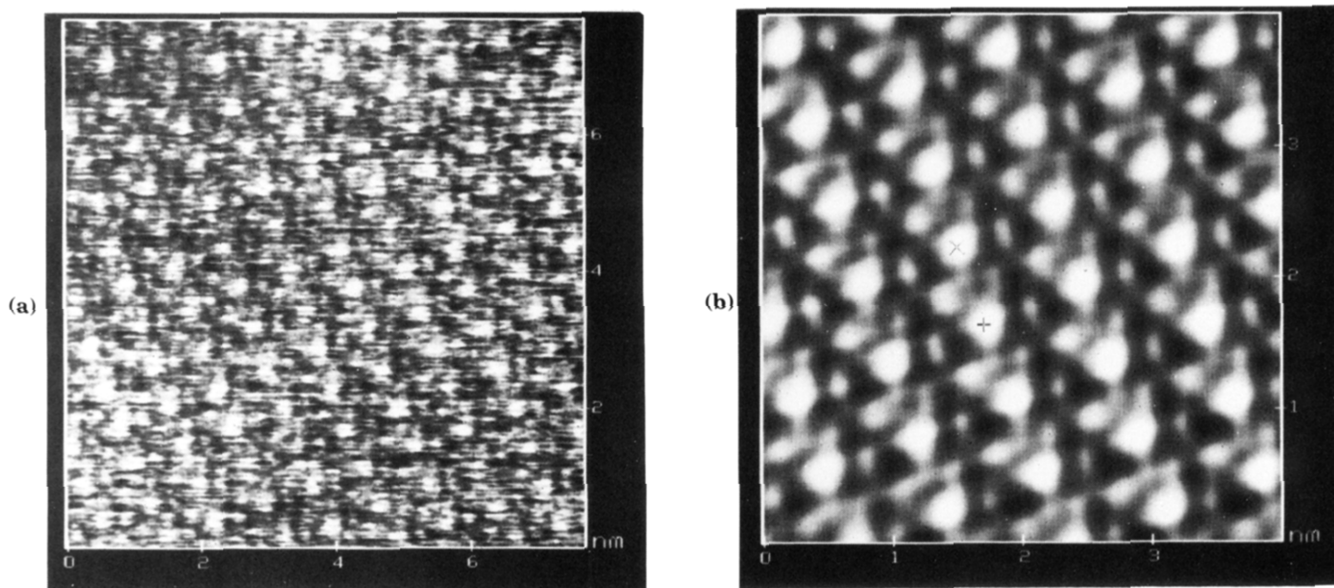

Figure 11. (a) STM current image recorded for the *bc* plane of $NbSi_{1/2}Te_2$ (I_{tun} = 1.8 nA, V_{bias} = 200 mV). (b) Zoomed part of the image in (a) after FFT filtering. The contrast covers the variations proportional to ln(*I*), where *I* is the tunneling current.

latter can also be explained if there is a slight height reconstruction in the surface Te-atom sheet.

$NbSi_{1/2}Te_2$. The height corrugation of the surface Te atom sheet is very small (Figure 2c), so that all Te atoms have a nearly equal density in the $\rho(r_0)$ plot (Figure 13a). To a lesser extent, this is also true in the $\rho(r_0,e_f)$ plot (Figure 13b). However, both in the AFM images (Figure 12) and in the STM images (Figure 11), one of the four surface Te atoms of a unit cell is brighter than the remaining three. This suggests a slight height reconstruction in the surface Te atom sheet. Though not shown, the $\rho(r_0,e_f)$ plot calculated by employing the levels at the conduction band bottom is very different in pattern from that shown in Figure 13b. For instance, the electron densities are not centered at the atomic positions. This is in support of our rigid band description of Si-deficient samples.

Concluding Remarks

For layered transition chalcogenides and halides with no interlayer distances shorter than van der Waals contacts, our earlier studies show[10] that the STM and AFM images are respectively well described by the $\rho(r_0,e_f)$ and $\rho(r_0)$ plots calculated from their bulk crystal structures. For all three compounds $NbGe_{2/5}Te_2$, $NbGe_{1/3}Te_2$, and $NbSi_{1/2}Te_2$ discussed above, however, the contrast patterns of the AFM and STM images can be satisfactorily explained only if one assumes a slight height reconstruction in the surface Te-atom sheet. This conclusion is not surprising because they have interlayer Te···Te contacts much shorter than the van der Waals radii sum. The cleavage of these contacts at the surface might induce a slight relaxation of the positions of the surface Te atoms. In addition, a surface corrugation can be induced by the forces exerted from the tip according to the local hardness of the surface Te atom sheet.[12]

The STM and AFM images of commensurate phases $NbGe_{2/5}Te_2$, $NbGe_{1/3}Te_2$, and $NbSi_{1/2}Te_2$ are all characterized by a pseudohexagonal arrangement of spots representing the surface Te atoms, if their contrast dif-

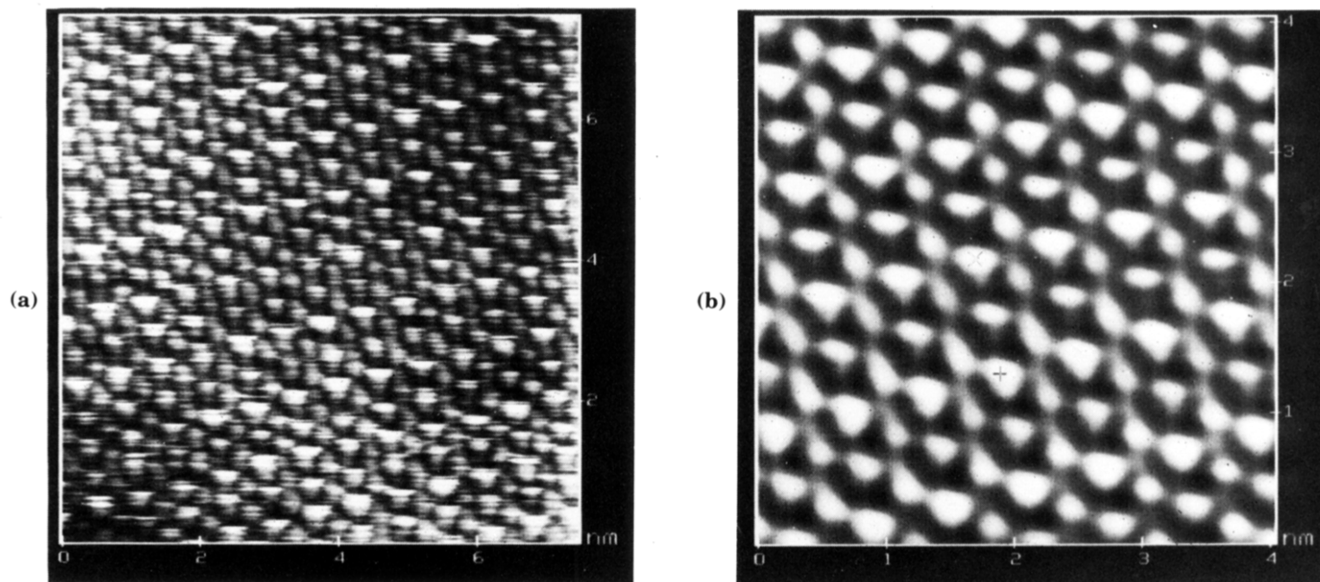

Figure 12. (a) AFM image recorded for the *bc* plane of $NbSi_{1/2}Te_2$. (b) Zoomed part of the image in (a) after FFT filtering. The contrast covers the height variations in the 0.0–1.1-nm range in (a) and (b).

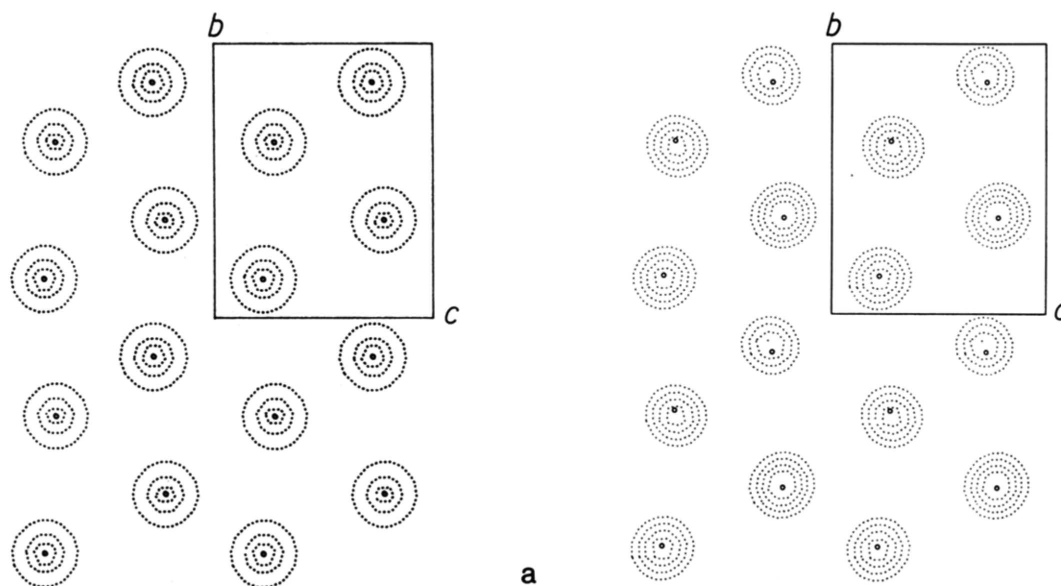

Figure 13. (a) $\rho(r_0)$ plot calculated for the *bc* plane of $NbSi_{1/2}Te_2$. The contour values are 0.25, 0.20, and 0.10 × 10^{-1} electron/au^3. (b) $\rho(r_0,e_f)$ plot calculated for the *ac* plane of $NbSi_{1/2}Te_2$. The contour values are 0.60, 0.40, and 0.20 × 10^{-3} electron/au^3.

ferences are neglected. The surface unit-cell parameters of these commensurate MA_xTe_2 phases are well reproduced by STM and AFM. Thus, it seems likely that STM and AFM can be used to characterize the nature of incommensurate MA_xTe_2 phases.

Acknowledgment. The work at North Carolina State University (NCSU) was supported by the Office of Basic Energy Sciences, Division of Materials Sciences, U.S. Department of Energy, under Grant DE-FG05-86ER45259, which made it possible for S.N.M. to visit NCSU.